Table 2
VOCs recoveries (%) using the domestic standard cartridge (Sibata-charcoal) at the outlet

Recovery (%)	50 °C	60 °C	70 °C	80 °C
1,1-Dichloroethylene	96.65	104.08	88.64	96.51
trans-1,2-Dichloroethylene	99.83	101.27	87.73	93.90
cis-1,2-Dichloroethylene	100.29	102.37	90.04	95.44
Chloroform	104.47	106.36	94.32	100.56
1,1,1-Trichloroethane	107.17	106.63	95.16	100.32
Carbon tetrachloride	107.99	103.95	94.21	98.25
1,2-Dichloroethane	103.05	101.62	92.89	97.17
Benzene	104.16	101.77	93.49	95.27
Trichloroethylene	106.99	102.99	95.16	99.75
1,2-Dichloropropane	105.43	109.92	92.99	96.29
Bromodichloromethane	107.14	101.92	95.54	99.88
cis-1,3-Dichloropropene	101.47	105.25	94.92	96.78
Toluene	105.04	107.66	96.08	96.86
trans-1,3-Dichloropropene	102.30	106.16	95.76	96.92
1,1,2-Trichloroethane	104.99	108.63	97.41	99.44
Tetrachloroethylene	104.88	108.92	96.72	100.63
Dibromochloromethane	101.32	109.19	97.23	99.60
m,p-Xylene	104.11	104.93	97.20	95.88
o-Xylene	102.58	102.88	96.08	94.99
Bromoform	101.48	104.78	97.04	106.39
p-Dichlorobenzene	87.53	88.24	90.70	91.61

771.7, 740.3, 274.1 and 178.6 μg/g, respectively. The HC-MWCNTs thus showed an affinity order of *p*-dichlorobenzene > *o*-xylene > *m,p*-xylene > toluene > benzene ≫ the other aliphatic VOCs.

3.4. Effects of temperature on aromatic VOCs adsorption

The effect of temperature on adsorption was studied for four aromatic VOCs (*m,p*-xylene, *o*-xylene, and *p*-dichlorobenzene), chosen as representative compounds. Experiments were conducted at 25, 40, 50, 60, and 70 °C, and the adsorptive capacity (μg VOCs per g HC-MWCNTs) for each compound was plotted against temperature (K) (Fig. 4). The adsorptive capacities for these VOCs decreased as the temperature increased. Moreover, an adsorption hill was observed for all four compounds at approximately 333 K. This feature was also observed for toluene

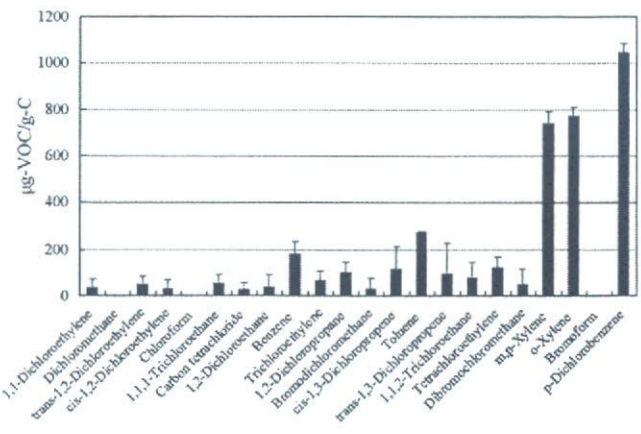

Fig. 3. Capacity of the HC-MWCNT-packed cartridges for adsorbing VOCs, expressed as micro-grams of VOCs per gram of HC-MWCNT.

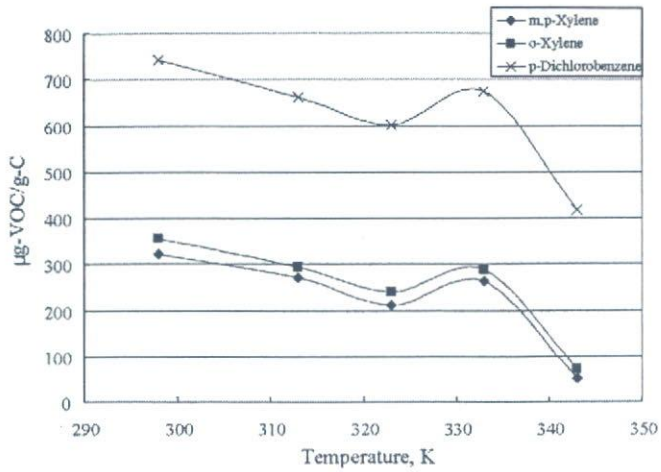

Fig. 4. Effects of adsorption temperature on the adsorptive capability of the HC-MWCNTs for VOCs.

and benzene, but was absent for the aliphatic VOCs (data not shown). The hills could be attributed to activated entry effects; *m,p*-xylene, *o*-xylene, and *p*-dichlorobenzene are disc-liked molecules [23]. Higher temperatures may facilitate diffusion of the aromatic VOCs, propelling the molecules through the tube/tube networks and enhancing the adsorptive capacity.

3.5. HOMO–LUMO interactions

The total energies of the highest occupied molecular orbital (HOMO) and the lowest unoccupied molecular orbital (LUMO) of the aromatic VOCs were calculated based on Fukui's frontier orbital theory [24,25] with a PM3 program. Table 3 summarizes the HOMO, LUMO, and LUMO–HOMO values. The *p*-dichlorobenzene had the highest HOMO energy (−9.459 eV), followed by *o*-xylene (−9.707 eV), *m*-xylene (−9.716 eV), toluene (−9.811 eV), and benzene (−10.945 eV). This sequence matches the order of the affinities of the aromatic VOCs for the HC-MWCNTs.

HOMO and LUMO electron densities for the aromatic VOCs were calculated using the MOPAC program (Fig. 5). The high frontier electron (HOMO) density points of the aromatic carbon atoms were C3 and C6 (0.3392, 0.3392) for *p*-dichlorobenzene, C1 and C6 (0.5080, 0.5082) for *o*-xylene, C3 and C6 (0.5663, 0.5663) for *p*-xylene, and C1 and C3 (0.4849, 0.5078) for *m*-xylene. The HOMO points for benzene were C1 and C4 (0.5429, 0.5429), and those for toluene were C3 and C6 (0.5960, 0.6118). The resulting HOMO electron density order was *p*-dichlorobenzene < *o*-xylene < *p*-xylene < benzene < toluene.

Table 3
HOMO, LUMO, and LUMO–HOMO energies of aromatic VOCs

VOCs	HOMO (eV)	LUMO (eV)	LUMO–HOMO (eV)
Benzene	−10.115	0.025	10.139
Toluene	−9.811	−0.069	9.742
m-Xylene	−9.716	−0.085	9.631
p-Xylene	−9.592	−0.105	9.487
o-Xylene	−9.707	−0.070	9.637
p-Dichlorobenzene	−9.459	−0.425	9.034

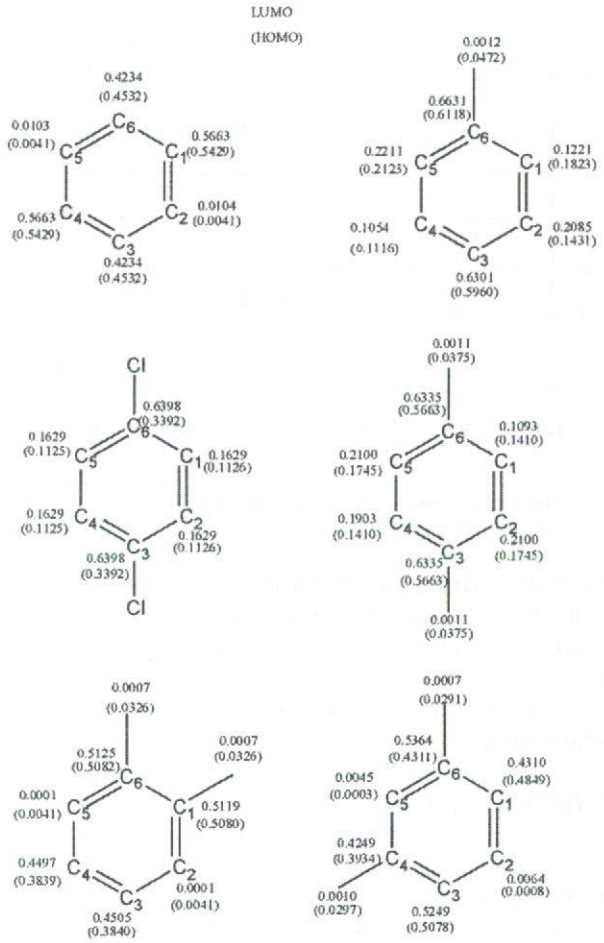

Fig. 5. Electron densities of HOMO and LUMO on the carbon atoms of the aromatic VOCs, calculated using the MOPAC program. Parentheses indicate HOMO values.

These calculations provide new insight into the mechanism of aromatic VOCs adsorption by HC-MWCNTs. The high degree of adsorption is due to the transfer of the π-electrons from the HOMO of the HC-MWCNTs to the LUMO of the aromatic VOCs. The *frontier* electrons (HOMO) of the aromatic VOCs, on the other hand, repel the π-electrons transferring to the LUMO. Therefore, a compound with a small HOMO–LUMO gap will have a higher affinity towards the HC-MWCNTs. For example, *p*-dichlorobenzene has the smallest HOMO–LUMO gap and was the most extensively adsorbed by the HC-MWCNTs. The order of the affinities of the aromatic VOCs for the HC-MWCNTs (*p*-dichlorobenzene > *o*-xylene > *m,p*-xylene > toluene > benzene) was identical to the order of the HOMO–LUMO gap values.

3.6. Comparison to "as-grown" CNTs

Fig. 6 shows the experimental data obtained using the as-grown MWCNTs and SWCNTs as adsorbents. The value of R (ratio of the intensity of the D band to that of G band) for the MWCNTs was 0.92. The specific surface area measured by N_2 adsorption (BET method) was 91 m^2/g. For the as-grown SWCNTs, $R = 1.86$ and the specific surface area was 254 m^2/g. The

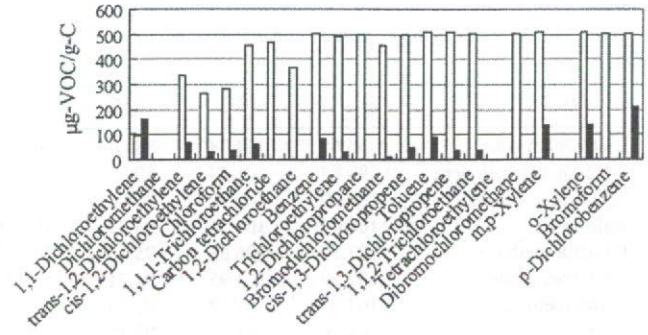

Fig. 6. Adsorptive studies carried out using the as-grown MWCNT-packed cartridge (white column) and the as-grown SWCNT-packed cartridge (black column) as the adsorbing media. Other experimental conditions were the same as for the HC-MWCNTs experiments.

selectivity/affinity for adsorbing the aromatic VOCs decreased and finally disappeared as the ratio of the crystalline to amorphous carbon decreased.

4. Conclusion

Carbon nanotubes with a highly crystalline structure have been demonstrated to be capable of selectively adsorbing aromatic VOCs. The affinity of a VOCs compound for MWCNTs was determined by both its LUMO and HOMO values. From the molecular orbital point of view, the adsorption of the aromatic VOCs by HC-MWCNTs can be considered a kind of "soft-chemical bonding" interaction. Research is ongoing on the use of MWCNT-based adsorbents for the elimination of aromatic VOCs from indoor air.

Acknowledgements

This work was supported by funding from Grants-in-Aid for Scientific Research from the Ministry of Education, Culture, Sports, Science and Technology of Japan (No. 18310049), by the Japan Science and Technology Agency (JST), and by the Ministry of Health, Labor, and Welfare (No. H18-Chem-Gen-006).

References

[1] S.K. Brown, M.R. Sim, M.J. Abramson, C.N. Gray, Indoor Air 4 (1994) 123.
[2] S.O. Baek, Y.S. Kim, R. Perry, Atmos. Environ. 31 (1997) 529.
[3] P.O. Fanger, Indoor Air 10 (2000) 68.
[4] P. Wolkoff, G.D. Nielsen, Atoms. Environ. 35 (2001) 4407.
[5] L.A. Wallace, E.D. Pellizzari, T.D. Hartwell, V. Davids, L.C. Michael, R.W. Whitmore, Environ. Res. 50 (1989) 37.
[6] L.A. Wallace, W. Nelson, R. Ziegenfus, E. Pellizzari, L. Michael, R. Whitmore, H. Zelon, T. Hartwell, R. Perritt, J. Expos. Anal. Environ. Epidemiol. 1 (1991) 157.
[7] D. Das, V. Graur, N. Verma, Carbon 42 (2004) 2949.
[8] M. Peng, L.M. Vane, S.X. Liu, J. Hazard. Mater. B98 (2003) 69.
[9] M.R. Tancerde, W.L. Zeise, E.A. Crouch, Atoms. Environ. 21 (1987) 2187.
[10] J. Begerow, E. Keles, T. Koch, L. Dunemann, J. Chromatogr. A 749 (1996) 181.
[11] M.J. Ruhl, Chem. Eng. Prog. 89 (1993) 37.

[12] M.A. Lillo-Rodenas, D. Cazorla-Amoros, A. Linares-Solano, Carbon 43 (2005) 1758.
[13] J.H. Byeon, J.H. Park, K.Y. Yoon, B.J. Ko, J.H. Ji, J. Hwang, Carbon 44 (2006) 2089.
[14] M.S. Dresselhaus, G. Dresselhans, P.C. Ekiund, Science of Fullerenes and Carbon Nanotubes, Academic Press, 1996.
[15] S. Iijima, Nature (Lond.) 354 (1991) 56.
[16] D.S. Bethune, C.H. Kiang, M.S. de Vries, G. Gorman, R. Savoy, J. Vasques, R. Breyers, Nature 363 (1993) 605.
[17] R.Q. Long, R.T. Yang, J. Am. Chem. Soc. 123 (2001) 2058.
[18] Q. Li, D. Yuan, Q. Lin, J. Chromatogr. A 1026 (2004) 283.
[19] E. Diaz, S. Ordonez, A. Vega, J. Colloid Interface Sci. 305 (2007) 7.
[20] M. Endo, M. Shikata, Jpn. J. Appl. Phys. 54 (1985) 507.
[21] M. Endo, Chem. Technol. 18 (1988) 568.
[22] Y.A. Kim, T. Hayashi, M. Endo, Y. Kaburagi, T. Tsukada, J. Shan, K. Osato, S. Tsuruoka, Carbon 43 (2005) 2243.
[23] Y. Chiang, P. Chiang, C. Huang, Carbon 39 (2001) 523.
[24] K. Fukui, T. Yonezawa, H. Shingu, J. Chem. Phys. 20 (1952) 722.
[25] K. Fukui, Acc. Chem. Res. 4 (1971) 57.

Journal of
Biomedical Nanotechnology
Vol. 3, 285–288, 2007

Multi-Walled Carbon Nanotubes Interact with Cultured Rice Cells: Evidence of a Self-Defense Response

Xiao-ming Tan and Bunshi Fugetsu*

Laboratory of Environmental Medical Chemistry, Graduate School of Environmental Science, Hokkaido University, Sapporo 060-0810, Japan

Multi-walled carbon nanotubes (MWCNTs) are widely used in nanotechnology despite concerns about possible toxic effects. To determine whether MWCNTs are toxic to rice, rice cells (*Oryza sativa L.*) were cultured with MWCNTs. Rice cells interacted with MWCNTs to form aggregates that were observed using light and scanning electron microscopy. Cell density decreased with increased MWCNT concentration, possibly indicating a self-defense response. Thus, MWCNTs interact directly with rice cells and may have a detrimental effect on rice growth. This effect, although, was stronger than that found for carbon blacks, the rice cells survived the MWCNTs through the self-defense response.

Keywords: Multi-Walled Carbon Nanotubes (MWCNTs), Rice (*Oryza sativa L.*) Cells, Non-Specific Interaction, Self-Defense Response.

1. INTRODUCTION

Developments in nanotechnology have led to predictions of great benefits as well as to warnings of great dangers to humanity and the environment. Carbon nanotubes (CNTs) have novel properties that are keys for many nanotechnology applications, and it is thought that tens or even hundreds of tons of CNTs will be produced worldwide within a few years.[1] This increase in CNT production will undoubtedly increase the exposure of humans and the environment to CNTs. A recent study found that the natural organic matter present in river water was capable of both stabilizing and dispersing CNTs.[2] Thus, if CNTs are toxic, their influence in the environment will be long lasting and could spread throughout the food chain. In fact, several studies on nanotoxicity have suggested that CNTs can adversely affect both humans and animals.[3–9] Bottini and co-workers evaluated the toxicity of pristine and oxidized multi-walled CNTs (MWCNTs) on human T cells.[3] They found that the latter are toxic and can induce massive loss of cell viability through programmed cell death at doses of 400 μg/ml, corresponding to approximately 10 million CNTs per cell. Muller et al. reported that Sprague–Dawley rats develop inflammation and fibrotic reactions after 60 days of exposure to CNTs.[5] Toxicity studies have thus far focused on the responses of organisms and/or specialized animal and human cells to CNT exposure.

In this study, we investigated whether MWCNTs are toxic to plants, using one of the most important crops in the world, rice, as a representative example. Hundreds of tons of MWCNTs have been used worldwide, so their possible impact on agriculture is of great interest. Studies were carried out by culturing cell suspensions of rice in the presence of MWCNTs. Our results showed interactions between rice cell and MWCNTs and provided new insights into the rice self-defense system.

2. EXPERIMENTAL DETAILS

Mature rice embryos (*Oryza sativa L.*) were grown on Murashige and Skoog (MS) solid medium for callus induction.[10] After three months, established calli were separated from friable calli and transferred to AA liquid medium[11] for cell suspension culture. After ten days, MWCNTs were added to the AA liquid medium and dispersed by ultra-sonication. Three groups of five 10 ml samples were prepared: Group A had 0.05 g/l MWCNTs, Group B had 0.1 g/l MWCNTs, and Group C, the control, had no MWCNTs. These three groups of five samples were placed on a rotary shaker at 120 rpm in the dark. After 4 days of incubation, the samples were examined using light microscopy; cell density was also determined using an hemocytometer. For density determination, the cells in each sample were counted five times, and the greatest and smallest values ignored. Three values were thus used to determine the average density for each sample.

*Author to whom correspondence should be addressed.

 1550-7033/2007/3/285/004 doi:10.1166/jbn.2007.035

Table I. Dimensions and surface area of MWCNTs and carbon blacks used in this study.

Carbon materials	Dimensions	Surface area
MWCNT	20–40 nm × 0.50–50 μm	3.14×10^{-2}–6.28 μm^2
Carbon black	ϕ100–200 nm	0.031–0.126 μm^2

Comparison studies were conducted using carbon blacks (these partial-like materials have been the industrially utilized structural or conductive filler in plastics) as the reference samples. Table I summarizes the physical dimensions and the surface area. The surface area was calculated as either cylinders (MWCNTs) or spheres (carbon blacks). The possible reminded catalytic metals in the samples were removed by refluxing the carbon nano-materials in 4 M hydrochloric acid for approximately 20 hours.[12]

3. RESULTS AND DISCUSSION

The cell density in Groups A and B was much lower than in control Group C (Table II). Moreover, as the concentration of MWCNTs increased from 0.05 g/l to 0.1 g/l (two-fold), the cell density was reduced from 38 to 27 (71%). Light microscopy revealed many black clumps in the samples in Groups A and B, as well as cells that were not associated with MWCNTs (Fig. 1). Scanning electron microscopy (SEM) images confirmed that these black clumps were MWCNTs that were tightly wrapped around and associated with the cells (Fig. 2). The number and the size of the black clumps in sample B were much greater than in sample A, and the percentage of the area of the cells covered by MWCNTs ranged from 0 to 100%; in some instances, the covered area was greater than 100% due to multiple layers of MWCNTs (see Fig. 1). It also seemed that once cells were associated with MWCNTs, further association was more likely until finally an aggregate or precipitate formed. In other words, when MWCNTs were added to the culturing solution, all the cells in suspension would theoretically have an equal probability of making contacting with them. However, only part

Table II. The effects of MWCNTs on the density of cultured rice cells grown in suspension. Carbon blacks were used as the reference for comparison.

Density cells/1 μl	1	2	3	4	5	Average density
Group A[a]	45	41	36	38	29	38
Group B[b]	25	78	28	15	28	27
Group R1[c]	52	31	50	34	86	45
Group R2[d]	47	30	72	17	32	36
Group C[e]	69	31	93	65	130	76

[a]Group A: 0.05 g/L MWCNTs. [b]Group B: 0.10 g/L MWCNTs. [c]Group R1: 0.05 g/L carbon blacks. [d]Group R2: 0.1 g/L carbon blacks. [e]Control samples (Group C): no MWCNTs. For each sample (5 samples/group), five density measurements were done. The largest and smallest values were ignored, and the three remaining values were used to calculate the average value (columns 1–5). These average values were used to calculate the average cell density for the group (rightmost column).

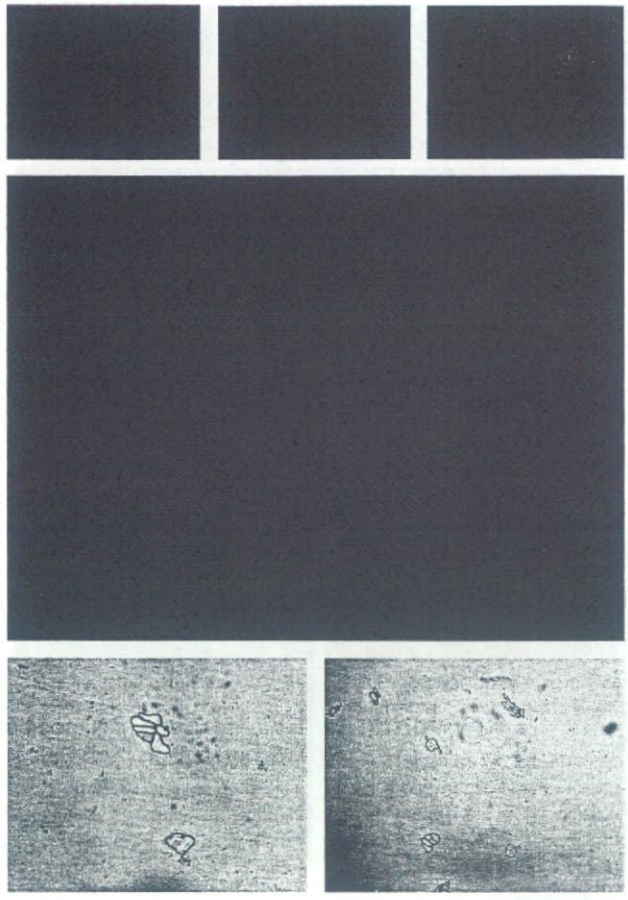

Fig. 1. Samples of cultured rice cells from Group A (0.05 g/L MWCNTs), B (0.10 g/L MWCNTs), and C (control; no MWCNTs) were examined at 200× magnification (excepted for the bottom right photo, which was100× magnification) by light microscopy. (A) The three upper images show cultured cells in a sample from Group A. Free cells and cells interacting with MWCNTs (black clumps) are visible. (B) The middle (expanded) image shows cultured cells in a sample from Group B. (C) The bottom images show cultured cells in a sample from control Group C.

of the cell population interacted with MWCNTs, and the cells that first associated with MWCNTs were then more likely to form even more associations until they were covered completely. As the cells combined with MWCNTs, the size of the cell/MWCNT aggregates (i.e., the black clumps) became larger until the aggregates were precipitated from the cell culture.

The reference materials, namely, carbon blacks have also shown some adverse effect; this, however, was smaller than MWCNTs. The cell density in Group R1 (carbon blacks, 0.05 g/l) and Group R2 (carbon blacks, 0.10 g/l) was 45 and 36 cell/1μl, respectively. On the other hand, for MWCNTs, the cell density was 38 and 27 cell/μl, respectively, under the identical situations. Very few black clumps (cells interacted with carbon black particles) were also observed, the percentage of the area of the cells covered by carbon blacks however, ranged from 0 to 20%.

In some sense, the cells in the aggregates played a protective role: Although some cells were sacrificed, their

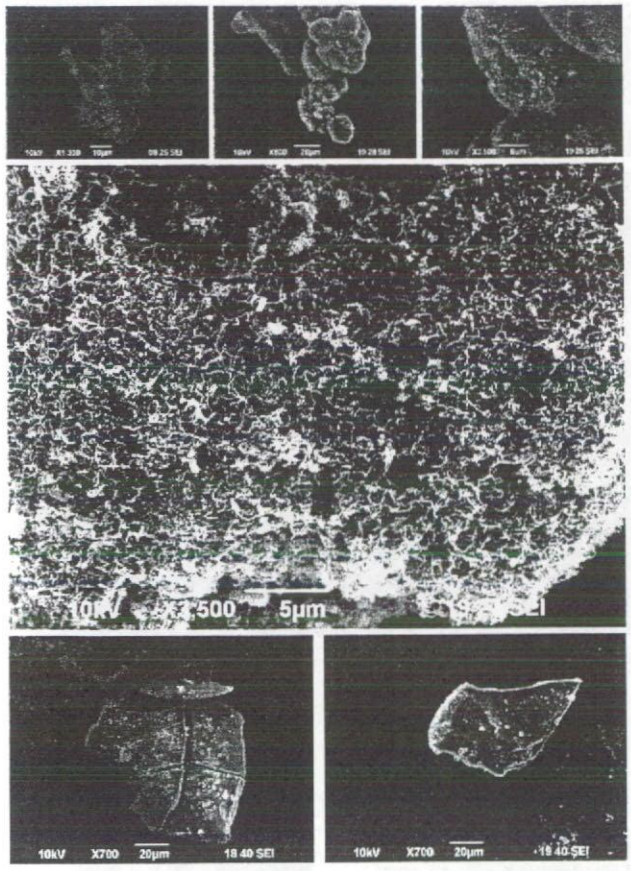

Fig. 2. Scanning electron microscopy was used to examine rice cells growing in the presence and absence of MWCNTs. (A) The three upper images and the middle (expanded) image show MWCNTs wrapped around rice cells, forming aggregates. (B) The bottom images show cells from control samples (Group C).

association with the MWCNTs made it less likely that other cells in the culture would interact with CNTs and also be precipitated. This effect can be viewed as a self-defense mechanism whereby a portion of the cell population is lost to save the rest of the culture from MWCNTs. It is known that plants have induced self-defense responses to a variety of biotic and abiotic stresses.[13–17] Biotic stresses include attack by herbivores and pathogens; abiotic stresses include factors such as atmospheric pollutants, light conditions, temperature variation, water availability, and salinity that can adversely affect plants. To protect themselves from stresses, plants can trigger the hypersensitive response, which results in the production of proteins or other organic chemicals that help them adapt to changes in the environment. For example, to protect themselves from viruses, plants create a zone of dead cells around an infection site that prevents the infection from spreading.[18]

The cell walls of plants are built up by harbor proteins and polysaccharides. It is possible that MWCNTs bind to certain proteins or polysaccharides, and that this binding causes a signaling cascade that results in strengthening of the cell walls due to increased production of proteins or polysaccharides. A recent study indicated that MWCNTs could alter protein expression in epithelial cells, which are the cells most affected by occupational exposure in nanotube manufacturing.[19] Another study used spectroscopic techniques to examine a composite formed by single walled carbon nanotubes and rice starch, and identified non-covalent interactions between the CNTs and the starch.[20] These two studies support the idea that CNTs can interact with certain proteins or polysaccharides. More experiments are needed to characterize the interaction between the cell wall and MWCNTs we observed in this study.

In conclusion, this study showed that rice cells can interact with MWCNTs in culture, and that this interaction results in a self-defense response by the rice cells. To the best of our knowledge, it is also the first study to investigate the possible impact of CNTs on plants. These preliminary experimental results show that MWCNTs pose a potential threat to rice at relatively high concentrations. Further studies will be needed to determine the impact of MWCNTs on rice growth and production.

Acknowledgments: This work was supported by funding from Grants-in-Aid for Scientific Research from the Ministry of Education, Culture, Sports, Science and Technology of Japan (No. 18310049), by the Japan Science and Technology Agency (JST), and by the Ministry of Health, Labor, and Welfare (No. H18-Chem-Gen-006).

References and Notes

1. P. Ball, Roll up for the revolution. *Nature* 414, 142 (**2001**).
2. H. Hyung, J. D. Fortner, J. B. Hughes, and J.-H. Kim, Natural organic matter stabilizes carbon nanotubes in the aqueous phase. *Environ. Sci. Technol.* 41, 179 (**2007**).
3. M. Bottini, Sh. Bruckner, K. Nika, N. Bottini, S. Bellucci, A. Magrini, A. Bergamaschi, and T. Mustelin, Multi-walled carbon nanotubes induce T lymphocyte apoptosis. *Toxicol. Lett.* 160, 121 (**2006**).
4. K. F. Soto, A. Carrasco, T. G. Powell, K. M. Garza, and L. E. Murr, Comparative *in vitro* cytotoxicity assessment of some manufactured nanoparticulate materials characterized by transmission electron microscopy. *J. Nanopart. Res.* 7, 145 (**2005**).
5. J. Muller, F. Huaux, N. Moreau, P. Misson, J. F. Heilier, M. Delos, M. Arras, A. Fonseca, J. B. Nagy, and D. Lison, Respiratory toxicity of multi-wall carbon nanotubes. *Toxicol. Appl. Pharmacl.* 207, 221 (**2005**).
6. G. Jia, H. Wang, L. Yan, X. Wang, R. Pei, T. Yan, Y. Zhao, and X. Guo, Cytotoxicity of carbon nanomaterials: Single-wall nanotube, multi-wall nanotube, and fullerene. *Environ. Sci. Technol.* 39, 1378 (**2005**).
7. D. B. Warheit, B. R. Laurence, K. L. Reed, D. H. Roach, G. A. Reynolds, and T. R. Webb, Comparative pulmonary toxicity assessment of single-wall carbon nanotubes in rats. *Toxicol. Sci.* 77, 117 (**2004**).
8. C. W. Lam, J. T. James, R. McCluskey, and R. L. Hunter, Pulmonary toxicity of single-wall carbon nanotubes in mice 7 and 90 days after intratracheal instillation. *Toxicol. Sci.* 77, 126 (**2004**).
9. N. A. Monteiro-Riviere, R. J. Nemanich, A. O. Inman, Y. Y. Wang, and J. E. Riviere, Multi-walled carbon nanotube interactions with human epidermal keratinocytes. *Toxicol. Lett.* 155, 377 (**2005**).

10. T. Murashige and F. Skoog, A revised medium for rapid growth and bioassays with tobacco tissue cultures. *Physiol. Plant* 15, 437 (**1962**).
11. K. Toriyama and K. Hinata, Cell suspension and protoplast culture in rice. *Plant Sci.* 41, 179 (**1985**).
12. F. Tian, D. Cui, H. Schwarz, G. Estrada, and H. Kobayashi, Cytotoxicity of single-wll carbon nanotubes on human fibroblasts. *Toxicol. Vitro.* 20, 1202 (**2006**).
13. J. Chen, E. Dawn, E. Hall, J. Murata, and V. De Luca, L-alanine induces programmed cell death in V labrusca cell suspension cultures. *Plant Sci.* 171, 734 (**2006**).
14. D. Ren, K.-Y. Yang, G.-J. Li, Y. Liu, and S. Zhang, Activation of Ntf4, a tobacco mitogen-activated protein kinase, during plant defense response and its involvement in hypersensitive response-like cell death. *Plant Physiology* 141, 1482 (**2006**).
15. H. Zhang, X. Zhang, Q. Li, and Z.-H. He, Alpha-picolinic acid activates diverse defense responses of salicylic acid-, jasmonic acid/ethylene- and Ca2+-dependent pathways in Arabidopsis and rice suspension cells. *Acta Botanica Sinica* 46, 1200 (**2004**).
16. Y. Ichinose, S. Andi, R. Doi, R. Tanaka, F. Taguchi, M. Sasabe, K. Toyoda, T. Shiraishi, and T. Yamada, Generation of hydrogen peroxide is not required for harpin-induced apoptotic cell death in tobacco BY-2 cell suspension culture. *Plant Physiol. Biochem.* 39, 771 (**2001**).
17. A. Cazalé, M. Rouet-Mayer, H. Barbier-Brygoo, Y. Mathieu, and C. Laurière, Oxidative burst and hypoosmotic stress in tobacco cell suspensions. *Plant Physiology* 116, 659 (**1998**).
18. Y. Liu, M. Schiff, K. Czymmek, Z. Tallóczy, B. Levine, and S. P. Dinesh-Kumar1, Autophagy regulates programmed cell death during the plant innate immune response. *Cell* 121, 567 (**2005**).
19. F. A. Witzmann and N. A. Monteiro-Riviere, Multi-walled carbon nanotube exposure alters protein expression in human keratinocytes. *Nanomedicine: Nanotechnolgy, Biology, and Medicine* 2, 158 (**2006**).
20. A. Casey, G. F. Farrell, M. McNamara, H. J. Byrne, and G. Chambers, Interaction of carbon nanotubes with sugar complexs. *Synth. Met.* 153, 357 (**2005**).

Received: 8 May 2007. Revised/Accepted: 12 June 2007.

Bio-Medical Materials and Engineering 18 (2008) 25–33
IOS Press

Bone tissue reaction of nano-hydroxyapatite/collagen composite at the early stage of implantation

N. Fukui [a,*], T. Sato [a], Y. Kuboki [b,c] and H. Aoki [d]

[a] *Department of Oral Health, School of Life Dentistry at Tokyo, The Nippon Dental University, Tokyo, Japan*

[b] *Department of Oral Health Science, School of Dental Medicine, Hokkaido University, Sapporo, Japan*

[c] *Koken Bioscience Institute, Tokyo, Japan*

[d] *International Apatite Co. Ltd., Tokyo, Japan*

Received 9 March 2007

Abstract. The purpose of this study was to develop a new biodegradable bone substitute materials consisting of synthesized nano-size hydroxyapatite (nano-HAp) and Type I biodegradable honeycomb collagen sponge (HCS) composites. Bone defects in rabbit mandibles were prepared by a drill, and the composites were implanted into the bone defects. The HCS only and the HCS/calcined hydroxyapatite (HAp) composite were used as comparative materials. The bone tissues reaction at the early stage within 3 weeks after implantaion was investigated histologically. Amounts of new bone formation were determined by NIH-image analysis software using the histological sections. The amounts of the new bone formation were largest in the nano HAp/HCS compared to the comparative materials. Within 2 weeks after implantation, the nano-HAp/HCS composite was more rapidly exchanged by new bone than the comparative materials.

From these results it was considered that the nano-HAp/HCS composites can be used as an effective biodegradable bone substitutive material.

Keywords: Nano-hydroxyapatite/honeycomb collagen sponge composite, bone tissue reaction, biodegradable

1. Introduction

Bone defect often occurs due to serious periodontal disease and cyst extraction. Regenerative therapy using tissue engineering in order to regenerate bone tissue lost for these reasons has become a topic of interest. When conducting regenerative therapy, various artificial materials for regeneration are required. Materials for regeneration must fulfill the following criteria: (1) act as a support for cells, (2) be capable of binding to biomolecules like cell growth factors, (3) be a geometrical factor, and (4) have biocompatibility [1,2].

On the other hand, hydroxyapatite (HAp), which is widely used as an artificial bone material, has excellent biocompatibility, absorbs strongly to protein, and has bone conductivity. In 1995 Li et al. [3]

*Address for correspondence: Naoto Fukui, Department of Oral Health, School of Life Dentistry at Tokyo, The Nippon Dental University, 1-9-20 Fujimi, Chiyoda-ku, Tokyo, 102-8159, Japan. Tel./Fax: +81 3 5996 0762; E-mail: naoto201@a.toshima.ne.jp.

reported that when hydroxyapatite nano-crystals was injected into bone marrow of rats, early osteogenesis in the bone marrow space was observed. Furthermore, in 1998 Li et al. [4] injected a milky HAp-sol into the upper first molar pulp of rats and reported there was little inflammatory response and that osteodentin was formed early on. It is believed that nano-HAp has inductivity related to the formation of hard tissue, however, no research has been conducted on its application in bone defect areas with the aim of bone tissue regeneration. When using nano-HAp as a bone implantation material, a carrier is needed which can keep the nano-HAp at the appropriate location.

In this study, we chose collagen as a scaffold developed by Koken Co. [5]. The collagen is an organic component of bone and an extracellular matrix (ECM), and has a number of important functions, including tissue binding and support, as well as the maintenance of differentiation, growth, and plasma of cell matrix liquid. Presently collagen is mainly used in tissue engineering, such as a scaffold in 3-D cells cultures and as a grafting material in biological systems [5,6]. A composite material was prepared with nano-HAp as a carrier prepared using ultrasonic homogenization of aqueous reaction solutions (a wet method) of phosphate and calcium ions and type I biodegradable honeycomb collagen sponge. Bone defects were artificially prepared in rabbit mandible, the defect as filled in with the nano-HAp/honeycomb collagen sponge composite, and the early stage of the bone tissue response examined histologically.

2. Materials and methods

2.1. Materials

2.1.1. Preparation of nano-HAp and calcined HAp

Nano-HAp was synthesized by adding dropwise an aqueous phosphate solution to a suspension of calcium hydroxide and then dispersing the mixture with an ultrasonic homogenizer with simultaneous stirring [9]. Physiological saline was added to this nano-HAp suspension to prepare 10% nano-HAp solution. The nano-HAp concentration was determined from the dry weight concentration measurement. The composition of the nano-HAp was analyzed by an X-ray diffractometry (XRD) and the morphology of the nano-HAp was observed using a transmission electron microscope (TEM). Calcined HAp was prepared by heating nano-HAp at 900°C for one hour.

2.1.2. Collagen

The honeycomb collagen sponge (HCS) used in the present experiment was the type I collagen which is present in a high amount in bone and developed by Koken Co. The collagen was low antigenic collagen pepsin-treated. For these reasons, it has low antigenicity and biodegradable property even when implanted into living tissue.

2.1.3. Preparation of composite material

Composite materials were prepared by soaking HCS in a nano-HAp suspension (nano-HAp/HCS group) or the calcined-HAp suspension (HAp/HCS group). All of the solutions were sterilized in an autoclave at 120°C. After the sterilization, the surface of each of the composite materials was examined with a scanning electron microscope (SEM). Composites containing 2%, 4%, 6%, 8% and 10% (weight %) of the nano-HAp or the HAp were prepared by using 10% HAp suspension. The amounts of the HAp was determined by a spectrophotometer according to the o-cresolphthalein complexone (OCPC) method.

2.2. Method

2.2.1. Animal experiment

Nine Japanese white rabbits (male, body weight 2.3–2.5 kg) were used. The rabbits were kept in a temperature-controlled room (24°C) with a 12 hour light–dark cycle and free access to solid pellet food and tap water during the experimental period. The implantation was carried out under anesthesia by an intravenous injection of 20 mg/kg of pentobarbital sodium. A dental drill together with a saline solution rinse was used to produce a cylindrical hole (diameter 2 mm; depth 4 mm) in the bottom edge of the mandible. A total of 6 holes were drilled, 3 on either side of the mandible. Two holes each were filled with collagen sponge and the two types of composite materials. The rabbits were given intramuscular injections of an antibiotic for three days after the surgical operation to prevent infection.

2.2.2. Preparation of histological specimens

The rabbits were sacrificed by an overdose of pentobarbital sodium at 1, 2 or 3 weeks after implantaion, and the bone tissue surrounding implants were excised from the mandible. The bone tissue was fixed in 10% formalin, dehydrated in 70% ethanol, decalcified for 3 days in formic acid then, embedded in paraffin. The tissue sections were stained with hematoxylin and eosin (H-E) and examined histologically under a light microscope.

2.2.3. Measurement of bone formation

The bone formation was determined by NIH-image analysis software using the tissue images by the light microscope at 1, 2 and 3 weeks after implantation. The percentage area (%) of new trabecula in the bone loss areas was calculated.

3. Results

3.1. Nano-HAp

A TEM image of the synthesized nano-HAp is shown in Fig. 1. The morphology and average size of the nano-HAp were needle and 10 nm wide and 50 nm long, respectively. XRD patterns of the nano-HAp (Fig. 2(A)) and HAp powder (Fig. 2(B)) are presented. Nano-HAp had low crystallinity compared to the HAp powder. The all patterns confirmed the both HAp were a typical hydroxyapatite crystal structure.

3.2. Composite materials

SEM images of the surfaces of HCS, nano-HAp/HCS and HAp/HCS are shown in Fig. 3. Pore sizes of HCS were 200–350 μm in Fig. 3(A) and (B). Adhesion of the nano-HAp on the surface of HCS was shown in Fig. 3(C) and (D). HAp powder with 2–9 μm in diameter on the surface of HCS were observed in the HAp/HCS in Fig. 3(E) and (F). The amounts of nano-HAp adsorbed in HCS are presented in Fig. 4. The nano-HAp adsorption weight ratio to HCS was different depending on the concentration of the nano-HAp suspension.

3.3. Histological findings

3.3.1. One week after implantation

Marked absorption of the collagen was not observed in any of the three groups. In the control group (HCS), a slight degree of round cell infiltration and fibrous connective tissue along HCS were observed

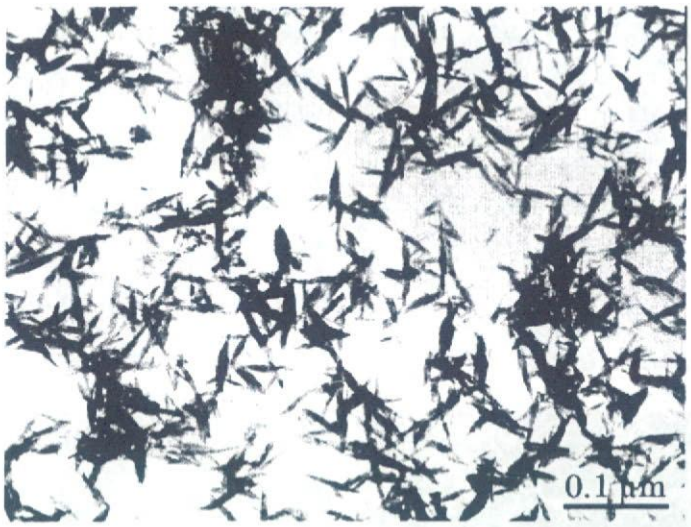

Fig. 1. Transmission electron microphotograph of Nano-HAp.

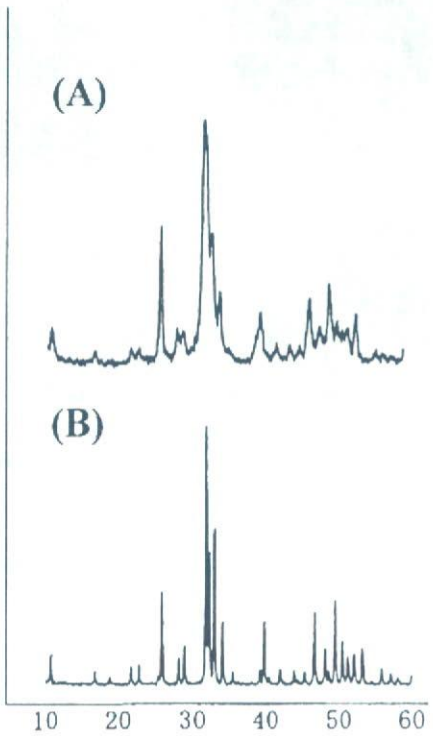

Fig. 2. XRD patterns of nano-HAp (A) and HAp calcined at 900°C (B).

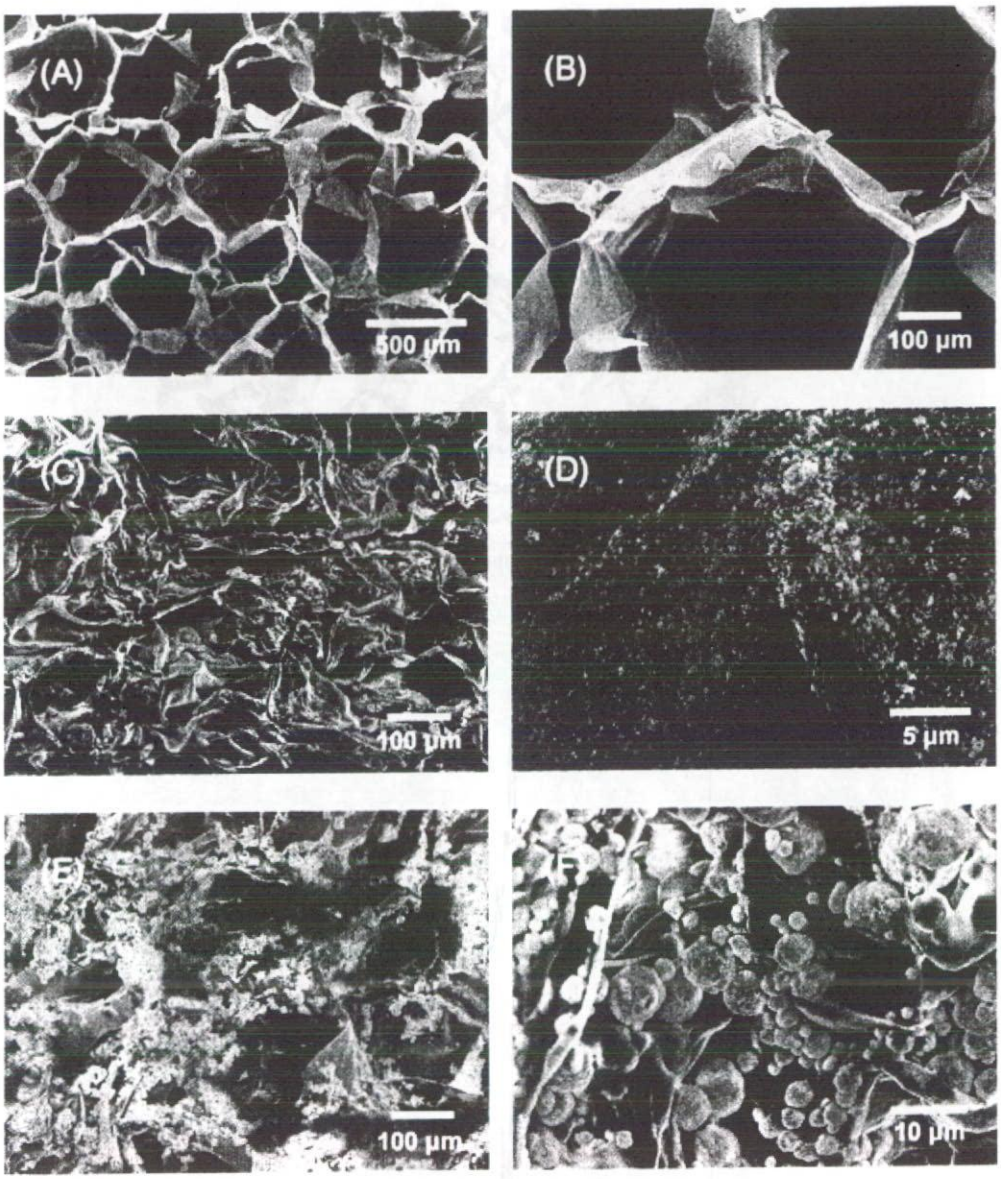

Fig. 3. Scanning electron microphotograph of HCS, Nano-HAp/HCS, HAp/HCS.

in Fig. 5(A). In the HAp/HCS group, the HAp powder and round cell infiltration were observed between HCS as seen in Fig. 5(B). In the nano-HAp/HCS group, young new bone formation from the host bone were observed in Fig. 5(C).

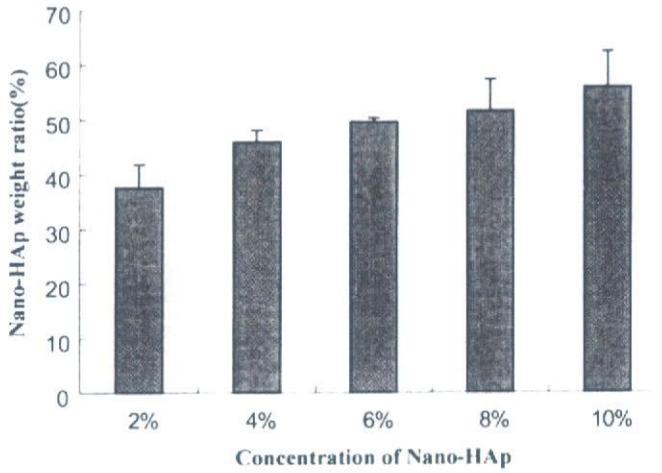

Fig. 4. Nano-HAp weight ratio (%) absorbed with HCS in 2–10% concentrations of nano-HAp suspension.

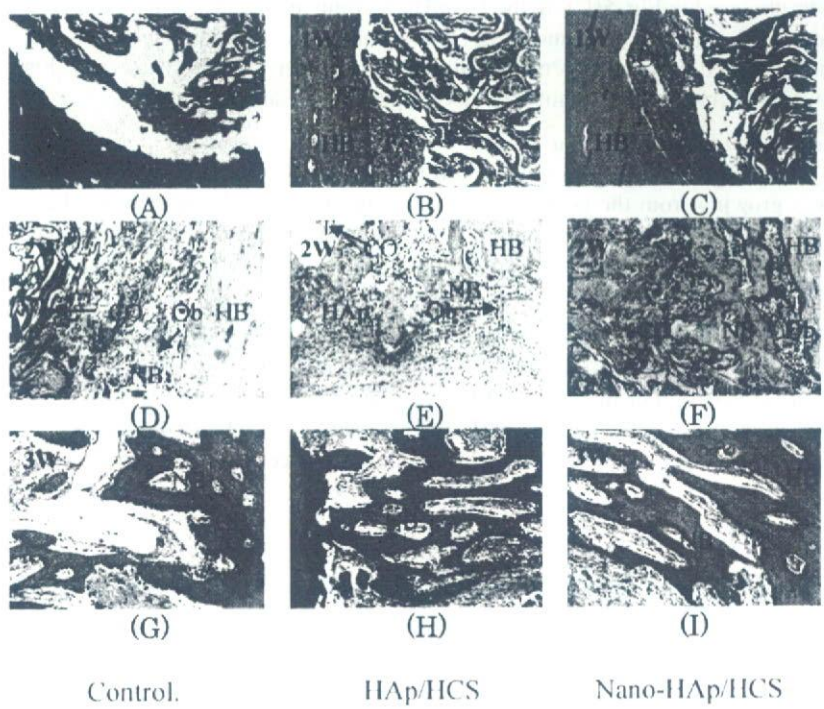

Fig. 5. Light microphotograph of HCS site after 1 week (A), 2 weeks (B), 3 weeks (C), HAp/HCS site after 1 week (D), 2 weeks (E), 3 weeks (F), Nano-HAp/HCS site, after 1 week (G), 2 weeks (H), 3 weeks (I) HB: host bone, NB: new bone, CO: HCS, FC: fibrous connective tissue, HAp: hydroxyapatite particle, Ob: osteoblast (× 100).

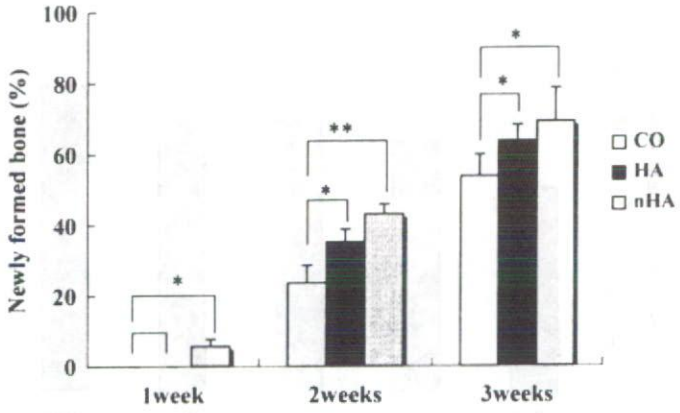

Fig. 6. Amounts of newly formed bone at 1, 2 and 3 weeks after implantation. CO: HCS, HA: HAp/HCS, nHA: nano-HAp/HCS. Solid bars with asterisk indicate statistical significance ($*P < 0.05$, $**P < 0.05$).

3.3.2. Two weeks after implantation

In the control group, some of HCS was remained without absorption and new bone formation along HCS wall was observed in Fig. 5(D). In the HAp/HCS group, new bone formation around HAp powder was observed in Fig. 5(E). In the nano-HAp/HCS group, some of the collagen was not absorbed and remained, and matured new bone formation along the collagen sponge was seen in Fig. 5(F). Active osteoblasts were observed in the vicinity of the collagen sponge and new bone.

3.3.3. Three weeks after implantation

The collagen sponge was completely absorbed by 3 weeks in all three groups. In the control group, new bone was growing from the host bone, however, the width of the new trabeculae was narrow as seen in Fig. 5(G). In the HAp/HCS group, comparatively narrow new bone was observed in Fig. 5(H). In the nano-HAp/HCS group, the formation of thick trabeculae was observed. It was also observed that the border between the host bone and new bone was indistinct Fig. 5(I).

3.3.4. Measurement of bone occupation ratio

The trabeculae occupation ratios are shown in Fig. 6. The ratios for the control group were 0% after one week, 23.6 ± 5.01% after two weeks, 53.7 ± 6.14% after three weeks, respectively. The ratios in the HAp/HCS group were 0% after one week, 36.7 ± 5.85% and 63.8 ± 4.56% after 3 weeks. In the nano-HA/HCS group, the ratios were 5.7 ± 2.15% after one week, 40.1 ± 2.75%, 69.2 ± 9.34% after 3 weeks, respectively.

4. Discussion

Nano-HAp has an excellent osteoinduction, however, it is suspension liquid, therefore, a scaffold material will be necessary as bone spacer. Honeycomb collagen sponge is multiporous, and cells and body fluids can infiltrate into it. Osteoblasts that have differentiated from undifferentiated mesenchymal stem cells of bone marrow use the implanted collagen sponge as a foothold, upon which osteoids are deposited, making bone formation occur more easily. The surface potential (zeta potential) of the nano-HAp is plus, while that of other HAp was minus [9]. It will be considered that this difference in surface

potential influences on protein adsorption characteristics, reaction with cells and osteogenesis. On the other hands, a honeycomb collagen sponge(HCS) has been used with the aim of providing scaffolding in three-dimensional cell cultures in tissue engineering.

From the points of view, we prepared a new composite materials composed of nano-HAp and HCS by immersing the HCA into the nano-HAP suspended in the physiological salt solution. Until now many papers of composite materials composed of collagen and HAp have been reported, however the crystal sizes of these HAp were more than 1 μm [11–14]. On the other hands, the sizes of the nano-HAp was less than 0.1 μm. The zeta potential of HAp more than 1 μm is negative, while the nano-HAp positive as mentioned in the paper reported by Aoki et al. In the present study, we were able to prepare, using a simple method in which a nano-HAp solution was adhered to a honeycomb collagen sponge carrier, a composite material with a 1:1 weight ratio. The composite material was prepared by simply dispersing nano-HAp in saline and then immersing the sol-form into collagen sponge. This method is simpler than existing procedures used until now. Amounts of new bone in the nano-HAp honeycomb group were greater than that in the collagen alone and HA honeycomb groups. Compared to HAp granules used thus far, the nano-size of nano-HAp granules is extremely fine so the surface area is greater which makes the surface potential plus, which in turn is believed to increase the adhesion efficiency of biomolecules, including cytokines such as bone morphogenetic proteins (BMPs), platelet-derived growth factor (PDGF), and transforming growth factor beta (TGF-b). It is conceivable that nano-HAp indirectly causes bone induction, without the introduction of cytokines, by adhering and accumulating cytokines. Furthermore, the rate of phagocytosis of nano-HAp by cells is large since nano-HAp are extremely minute [1]. Thus, it is thought the local concentrations of phosphate and calcium ions are increased and the activation of osteoblasts and other cells is promoted. In the field of dentistry, a material that can substitute for bone tissue when implanting an implant, etc., in order to achieve recovery of oral function following reconstruction of an area of bone loss is desirable. The composite discussed in the present study is believed to be an excellent substitute for early osteogenesis and autogenous bone.

5. Conclusion

A new biodegradable bone substitutive material was developed by combining synthesized nano-HAp and honeycomb collagen sponge. When the nano-HAp/collagen composite was implanted in areas of bone loss of rabbit mandible, the most rapid bone formation occurred surrounding the composite compared to the honeycomb collagen only or calcined HAp/the honeycomb collagen composite as comparative materials. The nano-HAp/collagen composite was more rapidly exchanged by new bone than collagen only or calcined HAp/collagen composite.

It was concluded that the nano-HAp/collagen composite can be used as an excellent biodegradable bone substitutive material.

References

[1] T. Iwakami and T. Imai, Effect of hydroxyapatite sol on cell proliferation and alkaline phosphatase activity of osteoblastic MC3T3-E1 cells, *Biomed. Mater. Eng.* **12**(3) (2002), 249–257.

[2] K. Ono, T. Yamamuro, T. Nakamura and T. Kokubo, Quantitative study on osteoconduction of apatite-wollastonite containing glass ceramic granules, hydroxyapatite granules, and alumina granules, *Biomaterials* **11**(4) (1981), 259–278.

[3] T. Li, K. Takigawa, M. Sakatsume and H. Aoki, Reaction of hydroxyapatite-sol in bone marrow, *Biomed. Mater. Eng.* **5**(2) (1995), 83–92.
[4] T. Li, M. Akao and M. Takagi, Tissue reaction of hydroxyapatite sol to rat molar pulp, *J. Mater. Sci.* **9** (1998), 643–649.
[5] H. Itoh, Y. Aso, M. Furuse, Y. Noishiki and T. Miyata, A honeycomb collagen carrier for cell culture as a tissue engineering scaffold, *Artif. Organs* **25**(3) (2001), 213–217.
[6] S. Mizuno, F. Allemann and J. Glowacki, Effect of medium perfusion on matrix production by bovine chondrocytes in three dimensional collagen sponges, *J. Biomed. Mater. Res.* **56**(3) (2001), 368–375.
[7] Y. Kuboki, M. Sasaki, A. Saito, H. Takita and H. Kato, Regeneration of periodontal ligament and cementum by BMP-applied tissue engineering, *Eur. J. Oral Sci.* **106** (1998), 197–203.
[8] K. Nemoto, H. Takita, R. Yoshimoto, J. George, T. Miyata and Y. Kuboki, Geometry of honeycomb collagen scaffold gives chamber-type micro-environmental units for ectopic osteogenesis when implanted with purified BMP cocktail into rat skin, *Tissue Eng.* **8** (2002), 1148.
[9] H. Aoki, *Medical Applications of Hydroxyapatite*, Ishiyaku EuroAmerica, Tokyo, St. Louis, 1988, pp. 176–180.
[10] H. Aoki, *Medical Applications of Hydroxyapatite*, Ishiyaku EuroAmerica, Tokyo, St. Louis, 1988, pp. 290–296.
[11] Y. Doi, T. Horiguchi, Y. Moriwaki, H. Kitago, T. Kajimoto and Y. Iwayama, Formation of apatite–collagen complexes, *J. Biomed. Mater. Res.* **31**(1) (1996), 43–49.
[12] A. John, L. Hong, Y. Ikada and Y. Tabata, A trial to prepare biodegradable collagen–hydroxyapatite composites for bone repair, *J. Biomater. Sci. Polym.* **12**(1) (2001), 689–705.
[13] E. Hahn, S. Sonis, G. Gallagher and D. Atwood, Preservation of the alveolar ridge with hydroxyapatite–collagen implants in rats, *J. Prosthesis Dent.* **60** (1988), 729.
[14] D.R. Mehlisch, T.D. Taylor, D.G. Leibold, R. Hiatt, D.E. Waite, P.D. Waite, D.M. Laskin, S.T. Smith and M.M. Koretz, Evaluation of collagen/hydroxyapatite for augmenting deficient alveolar ridges, a preliminary report, *J. Oral Maxillofac. Surg.* **45**(5) (1987), 408–413.

Differentiation of Mesenchymal Stem Cells Into Osteoblasts on Honeycomb Collagen Scaffolds

Joseph George,[1,2] Yoshinori Kuboki,[1] Teruo Miyata[1]

[1]Koken Bioscience Institute, 2-13-10 Ukima, Kita-ku, Tokyo 115-0051, Japan; telephone: +81-3-5914-2540; fax: +81-3-5914-2670; e-mail: jgeorge40@hotmail.com
[2]Division of Molecular Medicine, Department of Medicine, Columbia University, 630 West 168th Street, New York, NY 10032

Received 25 January 2006; accepted 13 March 2006

Published online 29 March 2006 in Wiley InterScience (www.interscience.wiley.com). DOI: 10.1002/bit.20939

Abstract: Tissue engineering using living cells is emerging as an alternative to tissue or organ transplantation. The adult mesenchymal stem cells can be differentiated into multilineage cells, such as adipocytes, chondrocytes, or osteoblasts when cultured with specific growth factors. In the present investigation, we have studied the effect of honeycomb collagen scaffolds for the adhesion, differentiation and proliferation of bone marrow-derived mesenchymal stem cells into osteoblasts. Mesenchymal stem cells were isolated from 6-week old albino rat femur bone marrow, and cultured in α-MEM medium without β-glycerophosphate and dexamethasone. Honeycomb collagen discs were prepared from bovine dermal atelocollagen, cross-linked by UV-irradiation and sterilized by heat. The honeycomb discs were placed on the culture dishes before seeding the stem cells. The cells attached quickly to the honeycomb collagen scaffold, differentiated and proliferated into osteoblasts. The differentiated osteoblasts were characterized by morphological examination and alkaline phosphatase activity. The osteoblasts also synthesized calcium-deficient hydroxyapatite (pseudo-hydroxyapatite) crystals in the culture. The mineralization was confirmed by Von Kossa staining and the crystals were analyzed by X-ray diffraction. Light microscopy and DNA measurements showed that the differentiated osteoblasts multiplied into several layers on the honeycomb collagen scaffold. The results demonstrated that the honeycomb collagen sponge is an excellent scaffold for the differentiation and proliferation of mesenchymal stem cells into osteoblasts. The data further proved that honeycomb collagen is an effective substrate for tissue engineering applications, and is very useful in the advancing field of stem cell technology and cell-based therapy. © 2006 Wiley Periodicals, Inc.

Keywords: tissue engineering; mesenchymal stem cells; osteoblasts; honeycomb collagen scaffold; cell based therapy

Correspondence to: Dr. Joseph George

Dr. Joseph George's present address is Division of Molecular Medicine, Department of Medicine, Columbia University, New York, NY 10032, USA.

INTRODUCTION

Tissue engineering is a developing branch of science that merges the fields of cell biology, molecular biology, bioengineering, material science, and surgery to provide new functional tissue using living cells, biomatrices and signaling molecules. Using this technology, tissue loss or organ failure can be treated by implantation of an engineered biological substitute, that is either functional at the time of implantation or has the potential to integrate and form the expected functional tissue at a later stage. The advantage of tissue engineering is that small biopsy specimens from relatively uninvolved sites can be obtained from the patient and cells can be isolated, cultured, and expanded into large numbers (Bruder and Fox, 1999; Levenberg and Langer, 2004; Mooney and Mikos, 1999; Service, 2005). Three dimensional (3-D) cell cultures on a bio-degradable cell scaffold is the basis of tissue engineering, where the specific cells can grow and multiply into a structure similar to tissue or organs in the living body (Holmes, 2002; Liu Tsang and Bhatia, 2004; Sutherland et al., 2005).

Maniatopoulos et al. (1988) first reported that bone marrow stromal cells obtained from young adult rats can differentiate into osteoblasts and express bone like structure when cultured with α-glycerophosphate and dexamethasone. Later it was proved that bone marrow derived non-hematopoietic mesenchymal stem cells (MSCs) are pluripotent and have the ability to differentiate into multilineage cells, to form a variety of mesenchymal tissues, including bone, cartilage, tendon, ligament, muscle, and adipose tissue which serve as a potential tool for tissue engineering (Ballas et al., 2002; Gregory et al., 2005; Kassem, 2004; Mauney et al., 2005; Pittenger et al., 1999). The MSCs can be easily isolated, purified, and expanded through 3-D cell culture systems from animals and humans. Because of the ease of their isolation and their extensive differentiation potential, MSCs are among the first stem cell types to be introduced into the clinic. The differentiated MSCs such as osteoblasts or chondrocytes can be grown on a suitable 3-D cell scaffold to

form the shape of a particular organ, which would permit replacement or regeneration of a defective bone or cartilage.

It was reported that honeycomb collagen scaffold prepared from bovine dermal atelocollagen is a suitable carrier for various 3-D cell cultures and has immense potential in the field of tissue engineering (Itoh et al., 2001; Masuoka et al., 2005; Sato et al., 2003). The geometry of honeycomb collagen scaffolds provide a unique structure and environment for cell attachment and differentiation. The aim of the present investigation was to study the effect of the honeycomb collagen scaffold for the adhesion, proliferation, and differentiation of bone marrow derived mesenchymal stem cells into osteoblasts, and also to evaluate the use of honeycomb collagen scaffold for stem cell technology and tissue engineering applications.

MATERIALS AND METHODS

Preparation of Honeycomb Collagen Scaffolds

The honeycomb collagen scaffolds (discs) were prepared from highly purified bovine dermal atelocollagen. In brief, 1% atelocollagen solution in 1 mM HCl (pH 3.0) was poured into a clean polystyrene shallow tray up to a thickness of 12 mm. It was neutralized using ammonia gas evolved from 5% ammonia solution in a closed chamber for 20 h. During this process the collagen solution turned into a white gel and the honeycomb structure was generated. The pore diameter of the honeycomb collagen sponge was adjusted to 200–400 μm, which is suitable for the optimum adhesion and proliferation of mesenchymal stem cells. The pore size was controlled by changing the concentration of collagen solution and ammonia gas. The collagen gel was placed in running tap water for 72 h in order to remove the excess ammonia and salt produced during neutralization. It was rinsed in distilled water and lyophilized in a special slow process. The lyophilized honeycomb collagen was sliced as 1 mm thick sheets using a slicing machine (Omas, Italy). About 15 mm diameter discs were cut using a mechanical punch from the 1 mm sheet. It was cross-linked under UV irradiation at a dose of 550 $\mu w/cm^2$ for 40 min on each side. Then the honeycomb collagen discs were dried at 110°C for 30 min and sterilized at 121°C for 6 h. The heat dried and sterilized honeycomb collagen discs were tested for cytotoxicity and directly used for the mesenchymal stem cell differentiation studies.

Isolation and Culture of Mesenchymal Stem Cells on Honeycomb Collagen Scaffold

About 6-week-old male Wistar rats of the albino strain were used for the isolation of mesenchymal stem cells. National guidelines for the care and use of laboratory animals were observed. The animals were sacrificed by cervical dislocation, abdominal area was shaved including legs and cleaned with 70% ethanol. The muscles present in the femoral area were removed, and both femoral bones were collected under sterile conditions and placed in a beaker containing alpha modification of minimum essential medium (α-MEM) with a 10-fold higher concentration of antibiotics (Penicillin and Kanamycin) than that generally used in cell culture media. The femoral bones were cut at both ends using sterile scissors while being held with a forceps on a sterile surface. Using a 5 mL syringe fitted with 18 G needle, 5 mL of the α-MEM containing 10-fold concentration of antibiotics was passed through the bone, and the bone marrow stromal cells were collected in a 50 mL sterile conical flask. The femoral bone was washed four times with 5 mL of α-MEM in order to collect the maximum number of stromal cells. Bone marrow stromal cells contain pluripotent stem cells along with large amounts of hematopoietic cells. The cells were mixed gently and filtered through a 52 μm membrane filter to remove the bone chips present in the preparation. The filtrate was centrifuged at 3,000 rpm for 5 min. The cells were washed again with α-MEM with 10-fold concentration of antibiotics. The purified cells were finally dispersed in α-MEM with 15% fetal bovine serum containing 100 U/mL penicillin and 60 μg/mL kanamycin sulfate, but without β-glycerophosphate and dexamethasone. The density of the cells in the preparation was adjusted appropriately using a phase contrast microscope and the cells were plated in 6-well corning polystyrene cell culture dishes. A 15 mm diameter and 1 mm thick sterile honeycomb collagen disc was placed on each well prior to seeding the cells. A set of control cultures without honeycomb collagen discs were also prepared simultaneously. The cells along with the honeycomb collagen scaffold was incubated at 37°C over 5% CO_2 in a humidified atmosphere. The cells attached quickly attached to the cell culture dish as well as to the honeycomb collagen scaffold. The media was changed after 6 h in order to remove the non-viable cells.

The amount of culture media was reduced to 50% of normal volume in order to avoid floating the honeycomb collagen disc, and also to accelerate the proliferation of mesenchymal stem cells on the scaffold. The media was changed carefully every 48 h without disturbing the honeycomb collagen scaffold. The proliferating cells anchored the honeycomb collagen discs to the culture dishes within 7 days of placement. The extracellular matrix synthesized by the proliferating cells re-enforced the attachment of the collagen scaffold to the culture dish. When the collagen discs were firmly attached to the culture dish, the amount of culture media was increased to the normal level. The proliferated mesenchymal stem cells differentiated into osteoblasts on the honeycomb collagen scaffold. The differentiated osteoblasts were examined every 48 h using an Olympus phase contrast microscope attached with Olympus digital camera and photographed. A few dishes of both the control and honeycomb collagen disc cultures were harvested on days 14 and 21. All cultures were terminated on day 28.

Morphological Analyses

Von Kossa Staining

Von Kossa staining (Bonewald et al., 2003) was carried out to characterize the biological mineralization of differentiated

osteoblasts. The scaffold was removed and the cells and mineral deposit below the scaffold were washed twice with phosphate buffered saline (PBS). The culture dish with the mineral deposit was then fixed with 10% phosphate-buffered formalin for 10 min, washed once with distilled water and serially rehydrated from 100% to 95% to 80% ethyl alcohol to distilled water. The water was removed and 2% silver nitrate solution was added. Then the dish was exposed to direct sunlight for 20 min, after which the plate was rinsed with water. Sodium thiosulfate (5%) was added for 3 min, the plates were then rinsed in water and counter stained with acid fuchsin for 5 min. The plates were washed with deionized water, then twice with 95% ethyl alcohol and 100% ethyl alcohol and finally dried in air.

X-Ray Diffraction Analysis

The microcrystals synthesized by the differentiated osteoblasts on honeycomb collagen scaffold were characterized for the biological mineralization through X-ray diffraction analysis. The culture media was pipetted out and the microcrystals formed below the scaffold were air dried and powdered by grinding. The powder was analyzed using an X-ray diffractometer (Rint 5000 of Rigaku Co. Ltd., Tokyo, Japan) in order to determine the crystallinity of the hydroxyapatite-like powder and for the presence of other crystal phases. A few standard powder X-ray diffraction spectrums of the synthetic hydroxyapatite and biological minerals, such as bone and tooth, were used to characterize the minerals formed by the differentiated osteoblasts.

Biochemical Analyses

Determination of Hydroxyproline and Total Collagen Content of the Scaffold

In order to study the synthesis of total collagen by the differentiated osteoblasts on the honeycomb collagen scaffold, the hydroxyproline content in the scaffold was measured on days 0,14, 21, and 28 during the course of the investigation. The honeycomb collagen scaffold along with the osteoblasts and cell matrix was removed from the culture dish and gently washed in PBS. It was hydrolyzed in 6 N HCl for 20 h at 110 °C in screw capped corning glass tubes. A set of fresh honeycomb collagen scaffolds were used as test controls. After hydrolysis, the acid was evaporated to dryness using a vacuum evaporator along with a hot water bath. The procedure was repeated twice after rinsing with distilled water to ensure the complete removal of the acid from the preparation. Finally it was dissolved in 2 mL of distilled water and used for the determination of hydroxyproline according to the method of Woessner (1961). In brief, 0.1 mL of the preparation was made up to 1 mL with distilled water and mixed with 1 mL of freshly prepared chloramine-T solution and allowed to stand for 20 min. It was further mixed with 1 mL of 3.15 M perchloric acid and left for 5 min. Finally, 1 mL of freshly prepared *p*-dimethylaminobenzaldehyde was added and mixed well; and the mixture was incubated in a water bath at 60°C for 20 min. The absorbance of the solution was measured in a spectrophotometer (Hitachi U-2000) at 560 nm. The total collagen content was calculated by multiplying the hydroxyproline content by the factor 7.46 as postulated by Neuman and Logan (Neuman and Logan, 1950). The test control collagen content was deducted from the total collagen content of the experimental sample.

Alkaline Phosphatase Assay

The alkaline phosphatase (ALP) activity of the differentiated osteoblasts on the honeycomb collagen scaffold was measured in control and test cultures. A set of both control and test cultures were harvested on days 14, 21, and 28 and washed twice with PBS. The cell matrix along with the honeycomb collagen scaffold was collected in 2 mL of PBS with the help of a cell scraper. About 1 mL of the cell suspension containing 0.2% IGEPAL CA-630 (Sigma-Aldrich Co.), 10 mM Tris-HCl and 1 mM $MgCl_2$ (final concentrations), pH 7.4 was sonicated gently (Ultrasonic Disruptor, UD-201, Tomy Co., Ltd., Tokyo, Japan). It was centrifuged at 3,000 rpm for 5 min at 4 °C and the supernatant was collected. The alkaline phosphatase activity in the supernatant was determined using an ALP assay kit (Wako, Japan) with *p*-nitrophenyl phosphate as substrate, following the method of Garen and Levinthal (1960). A standard curve was prepared using *p*-nitrophenol. The alkaline phosphatase activity is expressed as milli units (mU)/μg DNA. One unit of alkaline phosphatase is the activity of enzyme, which hydrolyzes 1 μmol of *p*-nitrophenyl phosphate in 1 min at 37 °C under the conditions of the assay.

DNA Measurements

The DNA content in the above cell preparation was determined using Hoechst 33258 reagent (Polysciences, Inc., USA), which follows the fluorometric method of Labarca and Paigen (1980). In brief, 1 μg of Hoechst reagent in 0.05 M phosphate buffer containing 2.0 M NaCl was mixed with 100 μL of diluted sample. The resultant fluorescence was measured using a Hitachi F-2000 fluorescence spectrophotometer with excitation at 356 nm and emission at 458 nm. Denatured DNA from Salmon testes (Wako, Japan) was used as the standard.

Statistical Analysis

Arithmetic mean and standard deviation were calculated for the data. The control culture data were compared with the test culture data on different days using Student's *t*-test. The value of $P < 0.05$ was considered as statistically significant.

RESULTS

The results of the present investigation are demonstrated in Figures 1–6. The structure of the honeycomb collagen

DOI 10.1002/bit

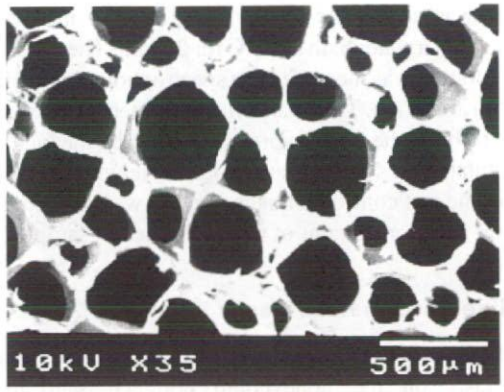

Figure 1. Scanning electron micrograph of a honeycomb collagen scaffold (×50).

scaffold prepared from the atelocollagen solution was studied by a scanning electron microscope (model JSM-5310LV, JEOL, Tokyo). Figure 1 demonstrates the scanning electron microscopic picture of the honeycomb collagen scaffold, which was cross-linked by UV-irradiation and stabilized by dry heat. As evident from the picture, the average pore size of the honeycomb collagen sponge was about 300 μm. Even though the honeycomb structure is biodegradable, it has the mechanical stability to hold the cells and did not fragment in the media during the culture period. The cross linking of collagen molecules by UV-irradiation during the preparation of the honeycomb structure helped to maintain the structural integrity of the scaffold. The structure of the scaffold was found to be very suitable for the proliferation, multiplication, and differentiation of mesenchymal stem cells into osteoblasts. The heterodimeric transmembrane glycoproteins such as integrins present on the cell surface carry negative charges, and the honeycomb collagen scaffold is positively charged. This opposite polarity would probably accelerate the quick attachment of the mesenchymal stem cells onto the collagen scaffold, which is a native extracellular matrix (ECM) protein.

The proliferation and differentiation of mesenchymal stem cells on honeycomb collagen scaffold is depicted on Figure 2.

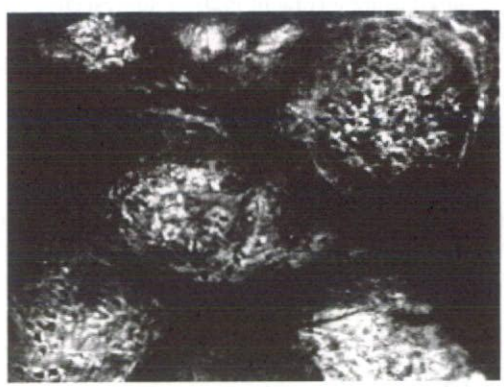

Figure 2. Proliferation of differentiated mesenchymal stem cells (osteoblasts) on a honeycomb collagen scaffold (×150). Day 14 after seeding the mesenchymal stem cells.

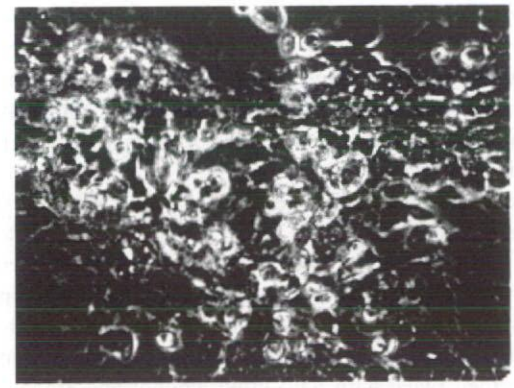

Figure 3. Low crystalline hydroxyapatite-like crystals (calcium-deficient hydroxyapatite) synthesized by the differentiated osteoblasts on a honeycomb collagen scaffold. Day 28 (×200). The image was taken using a phase contrast microscope after removing the honeycomb collagen disc from the culture for clearer visibility of the crystals.

The stem cells became spindle shaped within 24 h of plating. The spindle-shaped cells proliferated within the honeycomb structure, and slowly filled the honeycomb well. The entire honeycomb collagen scaffold was covered with differentiated osteoblasts by day 21 of culture. The synthesis of well-formed hydroxyapatite-like crystals by differentiated osteoblasts is demonstrated in Figure 3. Pure white crystals could be observed on day 28 inside the honeycomb collagen scaffold, as well as the surrounding area of the disc. Crystal formation was not observed in control cultures of mesenchymal stem cells without the honeycomb collagen scaffold. Von Kossa staining demonstrated dark brown colored nodular staining confirming the formation of minerals in the osteoblast cultures with honeycomb collagen scaffold. Von Kossa staining was negative in control cultures without the honeycomb collagen scaffold.

The X-ray diffraction spectrum of the microcrystals synthesized by the osteoblasts when cultured with honeycomb collagen scaffold is depicted in Figure 4. The powder X-ray diffraction pattern indicates a typical low crystalline hydroxyapatite similar to bone or dentine hydroxyapatite as seen in the Figure 4A with broad peaks. The chemical formula is represented as $Ca_{10}\text{-}xH_2x(PO_4)_6(OH)_2(x = 0\text{–}1)$, which is called a calcium deficient hydroxyapatite. On the other hand, the lower X-ray pattern with sharp peaks (B) indicates a typical stoichiometric hydroxyapatite, $Ca_{10}(PO_4)_6(OH)_2$ synthesized by a wet method using a calcium and phosphate ion solution reaction. The arrows in both figures indicate the characteristic peaks identified as hydroxyapatite.

The total collagen content synthesized by the differentiated osteoblasts during the culture on honeycomb collagen scaffold is presented in Figure 5. Synthesis of collagen is a characteristic feature of differentiated osteoblasts. Since honeycomb collagen scaffold is made up of 100% pure collagen, the total collagen synthesized by the differentiated osteoblasts is calculated by deducting the total collagen content of a fresh honeycomb collagen scaffold. A significant difference ($P < 0.001$) was observed in the total collagen